Frictional Figures of Merit for Single Layered Nanostructures

S. Cahangirov,[1,2] C. Ataca,[1,2,3] M. Topsakal,[1,2] H. Sahin,[1,2] and S. Ciraci[1,2,3,*]

[1]*UNAM-National Nanotechnology Research Center, Bilkent University, 06800 Ankara, Turkey*
[2]*Institute of Materials Science and Nanotechnology, Bilkent University, Ankara 06800, Turkey*
[3]*Department of Physics, Bilkent University, Ankara 06800, Turkey*

(Received 21 November 2011; revised manuscript received 20 January 2012; published 21 March 2012)

We determine the frictional figures of merit for a pair of layered honeycomb nanostructures, such as graphane, fluorographene, MoS_2 and WO_2 moving over each other, by carrying out *ab initio* calculations of interlayer interaction under constant loading force. Using the Prandtl-Tomlinson model we derive the critical stiffness required to avoid stick-slip behavior. We show that these layered structures have low critical stiffness even under high loading forces due to their charged surfaces repelling each other. The intrinsic stiffness of these materials exceeds critical stiffness and thereby the materials avoid the stick-slip regime and attain nearly dissipationless continuous sliding. Remarkably, tungsten dioxide displays a much better performance relative to others and heralds a potential superlubricant. The absence of mechanical instabilities leading to conservative lateral forces is also confirmed directly by the simulations of sliding layers.

DOI: 10.1103/PhysRevLett.108.126103 PACS numbers: 68.35.Af, 62.20.Qp, 81.40.Pq

Advances in atomic scale friction [1–3] have provided insight on dissipation mechanisms. The stick-slip phenomena is the major process, which contributes to the dissipation of the mechanical energy through sudden or nonadiabatic transitions between bistable states of the sliding surfaces [4–7]. During a sudden transition from one state to another, the velocities of the surface atoms exceed the center of mass velocity sometimes by orders of magnitudes [8]. Local vibrations are created and thereof evolve into the nonequilibrium system phonons via anharmonic couplings [9] within picoseconds [10]. In specific cases, even a second state in stick-slip can coexist [7].

In Fig. 1, two regimes of sliding friction are summarized within the framework of the Prandtl-Tomlinson model, [4,5,8] where an elastic tip (+cantilever) moves over a sinusoidal surface potential. The curvature of this potential at its maximum gives the value of the critical stiffness k_c. If the intrinsic stiffness of the tip k_s is higher than this critical stiffness, i.e., $k_s/k_c > 1$, the total energy of the tip-surface system always has one minimum. The sliding tip gradually follows this minimum, which results in the continuous sliding regime. Conversely, if the tip is softer than the critical value, then it is suddenly slipped from one of the bistable states to the other. This slip event can be activated by thermal fluctuations even before the local minimum point becomes unstable [11]. Experimentally, using a friction force microscope, Socoliuc *et al.*[12] showed that the transition from stick-slip regime to continuous sliding while attaining an ultralow friction coefficient can be achieved by tuning the loading force on the contact.

In this Letter, the sliding friction between two identical pristine layers of nanostructures, such as graphane [13,14], fluorographene [15,16], molybdenum disulfide [17], and tungsten dioxide [18], (abbreviated according to their stoichiometry as CH, CF, MoS_2, and WO_2, respectively) is investigated using the density functional theory [19]. We find that these nanostructures avoid stick-slip even under high loadings and execute continuous sliding. Consequently, the sliding occurs without the friction that would originate from the generation of nonequilibrium phonons. Our approach mimics the realistic situation, where the total energy and forces are calculated from first-principles as two two-dimensional (2D) layers undergo a 3D sliding motion under a constant (normal) loading force. This is the most critical and difficult aspect of our study. In this respect, our results provide a 3D

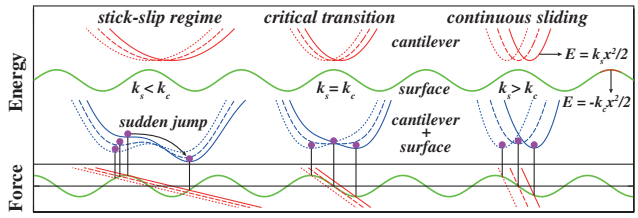

FIG. 1 (color online). Schematic representation of the stick-slip regime (left), critical transition (middle), and continuous sliding regime (right) in the Prandtl-Tomlinson model. Upper part: the potential energy curves of the surface (green [light gray] wavy line) and of the (tip + cantilever) (red [medium gray] lines); lower part: force variation of the surface (green [light gray] wavy line) and of the tip (red [medium gray] lines). Blue [dark gray] lines represent the potential energy of the tip and surface. The magenta dot shows the position of the tip on the surface, while its other end is positioned at the minimum of the parabola shown with red [medium gray] lines in the upper part. The dotted, dashed, and solid lines correspond to three different tip positions moving to the right.

rigorous *quantum mechanical* treatment for the 1D and empirical Prandtl-Tomlinson model [4,5].

The nanostructures considered in the present study are recently discovered insulators having honeycomb structure, which can form suspended single layers as well as multilayers. The unusual electronic, magnetic, and elastic properties of these layers have been the subject of recent numerous studies. In particular, they have large band gaps to hinder the dissipation of energy through electronic excitation and have high in-plane stiffness [16–18,20] [$C = (1/A)\partial^2 E_s/\partial\epsilon^2$, i.e., the second derivative of the strain energy relative to strain per unit area, A being the area of the unit cell]. Analysis based on the optimized structure, phonon and finite temperature molecular dynamics calculations demonstrate that each suspended layer of these nanostructures is planarly stable [14,16–18]. In graphane, positively charged three hydrogen atoms from the top side and another three from the bottom are bound to the alternating and buckled carbon atoms at the corners of hexagons in graphene to form uniform hydrogen coverage at both sides [See Fig. 2(a)]. Recently synthesized CF [15] is similar to CH, but F atoms are negatively charged. Tribological properties of carbon based fluorinated structures have been the focus of interest [21,22]. In the layers of MoS_2 or WO_2, the plane of positively charged transition metal atoms is sandwiched between two negatively charged outer S or O atomic planes. It was shown that MoS_2 structure can have ultralow friction [23]. Theoretically, the static energy surfaces are calculated during sliding at $MoS_2(001)$ surfaces [24]. Apparently, the interaction energy between two single layers of these nanostructures is mainly repulsive due to charged outermost planes except for very weak van der Waals attractive interaction around the equilibrium distance. In Fig. 2, each layer being a large 2D sheet consisting of three atomic planes mimics one of two sliding surfaces. In practice, sliding surfaces can be coated by these single layer nanostructures. Recently, this was achieved experimentally [25].

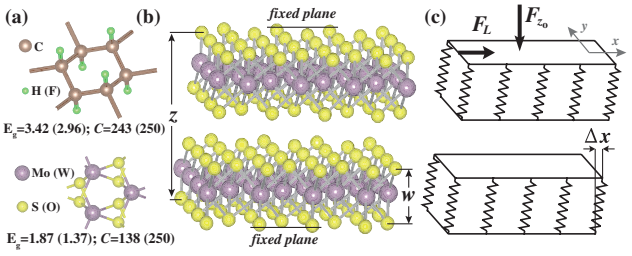

FIG. 2 (color online). (a) Ball and stick model showing the honeycomb structure of graphane CH (fluorographene CF) (top) and MoS_2 (WO_2) (bottom). Calculated values of energy gaps E_g and in-plane stiffness C are also given in units of eV and J/m^2, respectively. (b) Two MoS_2 layers sliding over each other have the distance z between their outermost atomic planes. (c) Each layer is treated as a separate elastic block. Lateral F_L and normal (loading) F_{z_0} forces, the shear of bottom atomic plane relative to top atomic plane in each layer $\Delta x(y)$, and the width of the layer w, are indicated.

We consider two layers of the same nanostructures in relative motion, where the spacing z between the bottom atomic plane of the bottom layer and the top atomic plane of the top layer is fixed. Here the frictional behavior of the system is dictated mainly by C-H(F), Mo-S, and W-O bonds and their mutual interactions. These layers are represented by periodically repeating rectangular unit cells. We calculate the value of the equilibrium lattice constants, which increases as z decreases. For each value of z the fixed atomic layer at the top is displaced by x and y on a mesh within the quarter of the rectangular unit cell. Then all possible relative positions (displacements) between fixed atomic layers are deduced using symmetry. At each mesh point all atoms of the system except those of fixed top and bottom planes are relaxed and the total energy of the system $E_T(x, y, z)$ (comprising both layers) is calculated. We have also derived $\Delta x(x, y, z)$ and $\Delta y(x, y, z)$ data which correspond to the shear (deflection) from the equilibrium position of the relaxed atomic planes relative to the fixed atomic plane of the same layer as illustrated in Fig. 2(c). The matrices of these data are arranged for each nanostructure using the mesh spacing of $\sim$0.2 Å in x and y directions. The forces exerting on the displacing top layer in the course of relative motion of layers are calculated from the gradient of the total energy of the interacting system, namely $\vec{F}(x, y, z) = -\vec{\nabla}E_T(x, y, z)$ at each mesh point (x, y). These forces are in agreement with the resultant of the atomic forces calculated for the top layer using Hellman-Feynman theorem. Eventually, the matrices of all data, namely $E_T(x, y, z)$, $\Delta x(x, y, z)$, $\Delta y(x, y, z)$, and $\vec{F}(x, y, z)$ are made finer down to a mesh spacing of $\sim$0.05 Å using spline interpolation.

The properties affecting the friction between layers should be derived under a given constant loading force. First of all we preset the value of applied loading, F_{z_0}, which corresponds to the operation pressure when divided by the cell area A, namely $\sigma_N = F_{z_0}/A$. We obtain the normal force from $F_z(x, y, z) = -\partial E_T(x, y, z)/\partial z$ and for each x and y we calculate the value of z where $F_z(x, y, z) = F_{z_0}$ and abbreviate it as $z_0(x, y)$. Then by using spline interpolation in the z direction we calculate the x and y dependence of $F_{x_0}[x, y, z_0(x, y)]$ and $F_{y_0}[x, y, z_0(x, y)]$, as well as $\Delta x_0[x, y, z_0(x, y)]$ and $\Delta y_0[x, y, z_0(x, y)]$ for a given F_{z_0}. The lateral force is then $\vec{F}_L[x, y, z_0(x, y)] = F_{x_o}\hat{i} + F_{y_0}\hat{j}$. Integrating the lateral force over the rectangular unit cell we obtain,

$$E_I[x, y, z_0(x, y)] = \int_0^x \int_0^y \vec{F}_L(x, y, z_0(x, y)) \cdot \vec{dr}$$

where $E_I[x, y, z_0(x, y)]$ is the interaction energy for displacement (x, y) in the cell under applied constant loading force F_{z_0}. It should be noted that E_I is different from

$E_T(x, y, z)$ (but $E_I \rightarrow E_T$ for $z \gg 1$) and is essential to reveal the friction coefficient. Contour plots of E_I of two sliding MoS_2 layers calculated for $\sigma_N = 15$ GPa are shown in Fig. 3(a) and those of CH, CF, WO_2 in Supplemental Material A [26]. The profile of E_I is composed of hills arranged in a triangular lattice. These hills correspond to the relative positions when the charged atoms of adjacent layers have the minimum distance. The hills are surrounded by two kinds of wells. The difference between these two wells is enhanced with increasing pressure. The wells form a honeycomb structure and are connected to each other through the saddle points (SPs). When the layers are moved over each other they will avoid the relative positions corresponding to the hills. For example, if the layers are pulled in the y direction they will follow the curved $F_x = 0$ path passing through the wells and SPs but not the straight one passing through the hills as shown in the Fig. 3(b). This makes the SP very important because in order to move from one well to the adjacent one, a barrier must be overcome at this point. We note that the critical stiffness can be calculated from the curvature of E_I^0, which is obtained by subtracting the strain energies of two sliding MoS_2 layers, namely $E_I^0 = E_I - k_s(\Delta x_0^2 + \Delta y_0^2)$ and by replacing x by $x - 2\Delta x_0$. While the SP serves as a barrier in the direction joining the nearby wells it acts as a well in the perpendicular direction joining the hills. Since we are interested in the curvature of the SP in the former direction we have made a plot along the $F_y = 0$ line which passes through the hill, the wells, and the SP in between as shown in the Fig. 3(b). We derive two critical stiffness values from the E_I^0 curve for a given normal loading force; namely k_{c1} at the SP and k_{c2} at the hill by fitting the curve at the maxima of the barriers to a parabola. Although the hills will be avoided during sliding motion the curvatures at these points are calculated for completeness. In Fig. 3(c) the variation of k_{c1} and k_{c2} of CH, CF, MoS_2, and WO_2 with loading pressure σ_N is presented. Generally, the critical stiffness, in particular k_{c1} is low due to repulsive interaction between sliding layers. This facilitates the transition to continuous sliding.

Next we calculate the intrinsic stiffness k_s of individual MoS_2 layers using the force and the displacement data. For each x and y the lateral forces $F_{x_0}[x, y, z_0(x, y)]$ and $F_{y_0}[x, y, z_0(x, y)]$ versus the displacements $\Delta x_0[x, y, z_0(x, y)]$ and $\Delta y_0[x, y, z_0(x, y)]$, respectively, are plotted. As shown in the inset of Fig. 3(b), this data falls on a straight line having a negative slope as expected from Hook's law of elasticity. We note that the elastic properties of layers having honeycomb structure are uniform and are independent of the direction of displacement and force [20]. The magnitude of the slope, $k_s = -F_{x(y)_0}/\Delta x(y)_0$ gives us the stiffness of the layers [27]. Calculated intrinsic stiffness values of CH, CF, MoS_2, and WO_2 in the range of σ_N from 5 GPa to 30 GPa are found to be

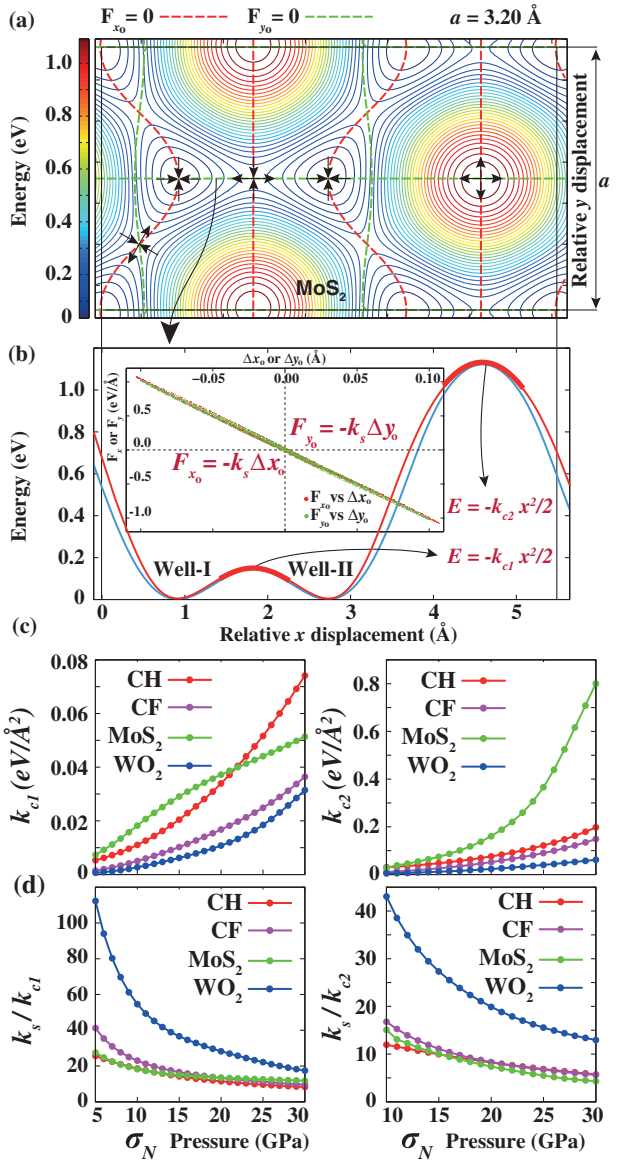

FIG. 3 (color online). (a) The contour plot of the interaction energy E_I of two sliding layers of MoS_2. The zero of energy is set to $E_I[0, 0, z_0(0, 0)]$. The energy profile is periodic and here we present the rectangular unit cell of it. The width of this unit cell in y direction is equal to the lattice constant a of the hexagonal lattice. Force in x (y) direction is zero along the red [medium gray] and green [light gray] dashed lines, respectively. There are several points at which the lateral force $\vec{F}_L$, is zero. The arrows at these critical points indicate the directions where the energy decreases. (b) The energy profiles of E_I (blue [dark gray] line) and E_I^0 (red [medium gray] line) along the horizontal line with $F_y = 0$ for MoS_2. The inset presents force versus shear values along x and y directions for each mesh point by red and green dots, respectively, which fall on the same line. Loading pressure in all cases is $\sigma_N = 15$ GPa. (c) The variation of k_{c1} and k_{c2} with loading pressure. (d) The variation of the ratios of k_s/k_{c1} and k_s/k_{c2}, i.e., frictional figures of merit with the loading pressure calculated for CH, CF, MoS_2, and WO_2.

6.15 ± 0.15 eV/Å^2, 4.5 eV/Å^2, 10.0 ± 0.3 eV/Å^2 and 15.2 ± 0.3 eV/Å^2, respectively. Clearly, these values of k_s, in particular those of MoS_2 and WO_2, are rather high.

Based on the discussion at the beginning, the ratios k_s/k_{c1} and k_s/k_{c2} give us a dimensionless measure of performance of our layered structures in sliding friction. When these ratios are above two (since both layers in relative motion contribute), the stick-slip process is replaced by continuous sliding, whereby the dissipation of mechanical energy through phonons is ended. Under these circumstances the friction coefficient diminishes, if other mechanisms of energy dissipation were neglected. For this reason one may call these ratios frictional figures of merit of the layered materials. In Fig. 3(d) we present the variations of the ratios k_s/k_{c1} and k_s/k_{c2} with normal loading forces. Even for very large σ_N, $k_s/k_{c1} > 2$ and $k_s/k_{c2} > 2$. For usual loading pressures, the stiffness of MoS_2, CF, and CH is an order of magnitude higher than corresponding critical values. Interestingly, for WO_2 this ratio can reach to two orders of magnitude at low pressures. The absence of mechanical instabilities has been also tested by performing extensive simulations of the sliding motion of layers in very small displacements. C-H, C-F, Mo-S and W-O bonds in each case of two layers in relative motion under significant loading force did not display the stick-slip motion.

Conversely, we now examine the sliding of two silicane [28] layers (abbreviated as SiH and composed of silicene [29] saturated by hydrogen atoms from both sides, like graphane) with $k_s = 2.1 \pm 0.1$ eV/Å^2 for 2 GPa $\leq \sigma_N \leq$ 8 GPa. This is an interesting material because the onset of stick-slip occurs already at low loading pressures and exhibits a pronounced asymmetry in the direction of sliding between two wells. In Fig. 4 we present the lateral force variation calculated for two different loading pressures. For small loading pressure, $\sigma_N = 2$ GPa the stick-slip motion is absent since approaching the SP from well I, the curvature is $k_{c,\mathrm{I}} = 0.28$ eV/Å^2 and from well II it is $k_{c,\mathrm{II}} = 0.16$ eV/Å^2, thus $k_s/k_{c,\mathrm{I\,or\,II}} > 2$ for both directions. Whereas, once the pressure is raised to $\sigma_N =$ 8 GPa stick-slip already governs the sliding friction, since

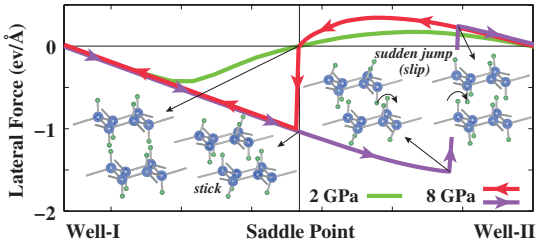

FIG. 4 (color online). Calculated lateral force variation of two single layer SiH under two different σ_N. The top layer is moving to the right or to the left between two wells. Atomic positions of two SiH layers in stick and slip stages are shown by the inset. The movement of SiH layers under the loading pressure of $\sigma_N =$ 8 GPa is presented in Supplemental Material B [31].

$k_{c,\mathrm{I}}$ reaches 1.38 eV/Å^2. Interestingly, since $k_{c,\mathrm{II}}$ is only 0.28 eV/Å^2 for $\sigma_N = 8$ GPa, going from well II to well I a slip event occurs at SP. Eventually, one sees in Fig. 4 a hysteresis in the variation of F_L leading to energy dissipation.

Earlier, the sliding motion of the diamondlike carbon (DLC) coatings exposed to hydrogen plasma resulted in a very low friction coefficient [30]. Ultralow friction was attributed to repulsive Coulomb forces between DLC films facing each other in sliding. However, when exposed to open air in ambient conditions, positively charged H atoms were replaced by negatively charged O and hence the uniformity in the charging was destroyed. In the present study, graphane coating is reminiscent of the hydrogenated DLC and accordingly is found to have ultralow friction, but vulnerable to degradation by oxygen atoms. Unlike graphane coating, WO_2 coating consists of negatively charged oxygen atoms and hence immune to oxidation.

In conclusion, using a criterion for the transition from the stick-slip to dissipationless continuous sliding regime, which is calculated from the first-principles, we showed that two sliding layered nanostructures, such as CH, CF, MoS_2, and WO_2, execute continuous sliding with ultralow friction. The minute variation of the amplitude of the interaction potential due to the repulsive interaction, as well as stiff C-H(F), Mo-S, and W-O bonds, underlie the ultralow friction predicted in the present study. Our predictions put forward an important field of application, ultralow friction coating for the layered honeycomb structures, which can be achieved easily to hinder energy dissipation and wear in sliding friction.

This work is supported by TUBITAK through Grant No. 108T234 also by EFS EUROCORE programme FANAS. All the computational resources have been provided by TUBITAK ULAKBIM, High Performance and Grid Computing Center (TR-Grid e-Infrastructure).

*ciraci@fen.bilkent.edu.tr

[1] C. M. Mate *et al.*, Phys. Rev. Lett. **59**, 1942 (1987).
[2] B. N. J. Persson, *Sliding Friction: Physical Principles and Applications* (Springer, Berlin, 1998).
[3] M. Urbakh and E. Meyer, Nature Mater. **9**, 8 (2010).
[4] L. Prandtl, Z. Angew. Math. Mech. **8**, 85 (1928).
[5] G. A. Tomlinson, Philos. Mag. **7**, 905 (1929).
[6] D. Tomanék, W. Zhong, and H. Thomas, Europhys. Lett. **15**, 887 (1991).
[7] A. Buldum and S. Ciraci, Phys. Rev. B **55**, 2606 (1997).
[8] M. H. Mueser, M. Urbakh, and M. O. Robbins, Adv. Chem. Phys. **126**, 187 (2003).
[9] V. L. Gurevich, *Transport in Phonon Systems* (North-Holland, Amsterdam, 1986).
[10] A. Buldum, D. M. Leitner, and S. Ciraci, Phys. Rev. B **59**, 16 042 (1999); H. Sevincli *et al.*, Phys. Rev. B **76**, 205430 (2007).
[11] E. Gnecco *et al.*, Phys. Rev. Lett. **84**, 1172 (2000).

[12] A. Socoliuc *et al.*, Phys. Rev. Lett. **92**, 134301 (2004).
[13] D. C. Elias *et al.*, Science **323**, 610 (2009).
[14] H. Şahin, C. Ataca, and S. Ciraci, Phys. Rev. B **81**, 205417 (2010).
[15] R. R. Nair *et al.*, Small **6**, 2877 (2010).
[16] H. Şahin, M. Topsakal, and S. Ciraci, Phys. Rev. B **83**, 115432 (2011).
[17] C. Ataca *et al.*, J. Phys. Chem. C **115**, 16 354 (2011).
[18] C. Ataca, H. Sahin, and S. Ciraci, J. Phys. Chem. C (to be published).
[19] We have performed first-principles plane-wave calculations within the generalized gradient approximation [J. P. Perdew, K. Burke, and M. Ernzerhof, Phys. Rev. Lett. **77**, 3865 (1996)] including van der Waals corrections [S. Grimme, J. Comput. Chem. **27**, 1787 (2006)] using PAW potentials [P. E. Blochl, Phys. Rev. B **50**, 17953 (1994)]. All structures have been treated within supercell geometry using the periodic boundary conditions. A plane-wave basis set with a kinetic energy cutoff of 400 eV and 500 eV is used for transition metal and carbon based structures, respectively. In the self-consistent potential and total energy calculations the BZ is sampled by $(10 \times 18 \times 1)$ for graphane and was scaled in this manner for other structures. All atomic positions and lattice constants are optimized by using the conjugate gradient method where total energy and atomic forces are minimized. The convergence for energy is chosen as 10^{-5} eV between two steps, and the maximum force allowed on each atom is less than 10^{-4} eV/Å. Numerical plane-wave calculations have been performed by using VASP [G. Kresse and J. Hafner, Phys. Rev. B **47**, 558 (1993); G. Kresse and J. Furthmüller, Phys. Rev. B **54**, 11169 (1996)].
[20] M. Topsakal, S. Cahangirov, and S. Ciraci, Appl. Phys. Lett. **96**, 091912 (2010).
[21] S. Miyake *et al.*, J. Tribol. **113**, 384 (1991).
[22] P. Thomas *et al.*, J. Phys. Chem. Solids **67**, 1095 (2006).
[23] J. M. Martin *et al.*, Phys. Rev. B **48**, 10 583 (1993).
[24] T. Liang *et al.*, Phys. Rev. B **77**, 104105 (2008).
[25] S. Chen *et al.*, ACS Nano **5**, 1321 (2011).
[26] See Supplemental Material A at http://link.aps.org/supplemental/10.1103/PhysRevLett.108.126103 for E_I profiles of CH, CF and WO_2 under $\sigma_N = 15$ GPa and variation of E_I^0 in MoS_2 with applied loading pressure.
[27] Note that, normally the stiffness is defined as stress over strain and has units of energy per volume. Here we only need the ratio of material stiffness to the critical stiffness and should have the same units. The critical stiffness was calculated as second order spatial derivative of energy in the unit cell and it has units of energy per unit cell per unit area. As defined above, the stiffness of layers, k_s, also has units of energy per unit cell per unit area.
[28] L. C. Lew Yan Voon *et al.*, Appl. Phys. Lett. **97**, 163114 (2010); M. Houssa *et al.*, Appl. Phys. Lett. **98**, 223107 (2011).
[29] S. Cahangirov *et al.*, Phys. Rev. Lett. **102**, 236804 (2009).
[30] A. Erdemir, Surf. Coat. Technol. **146**, 292 (2001).
[31] See Supplemental Material B at http://link.aps.org/supplemental/10.1103/PhysRevLett.108.126103 for the deformation and sudden jumps of SiH bonds during the stick-slip motion.